Stable and unstable surface evolution during the drying of a polymer solution drop

L. Pauchard and C. Allain*

Laboratoire FAST, Bâtiment 502, Campus Universitaire, Unité Mixte de Recherche Paris VI, Paris XI, CNRS UMR 7608, 91405 Orsay Cedex, France

(Received 5 May 2003; published 7 November 2003)

Drying of a sessile drop of a complex liquid can lead to intriguing complex shapes. We report here a study dealing with a model system, made of a hydrosoluble polymer that is glassy when pure. Under solvent evaporation, polymers accumulate near the vapor/drop interface and may form a glassy skin, which bends as the volume of liquid it encloses decreases. The conditions for the occurrence of this buckling instability have been investigated; the experimental results are well explained by a model that compares the characteristic times for drying and for the formation of a glassy skin. Depending on the experimental conditions, different types of shape distortion take place; secondary instabilities that break the axisymmetry are also observed.

DOI: 10.1103/PhysRevE.68.052801 PACS number(s): 83.80.Rs, 46.32.+x, 64.70.Pf, 62.10.+s

Classically investigated in structure engineering, for which shell and plate stability is of great importance [1], surface instabilities are also highly relevant to microscopic problems such as the crumbling of amphiphilic or biological polymerized membranes or the buckling-driven delamination of metallic films [2,3]. The surface stability is then determined both by the mechanical characteristics and by the physicochemical properties of the system and their time and space dependences. This is also the case for the buckling instability that we have recently observed during the drying of sessile drops of colloidal suspensions [4] or of polymer solutions [5,6]. Take a drying drop of a solution of a polymer which is glassy when pure: due to solvent evaporation, the outer layer of the drop is more concentrated in the polymer and may display a glassy transition. It then forms a ''skin'' that behaves like an elastic shell although it does not block the evaporation. This glassy skin will thus bend as the volume it encloses decreases, leading to large surface distortions.

In the present paper, we investigate experimentally the conditions under which drop surface buckling occurs and their dependence on the drying rate and contact angle. Our objective is particularly to examine the influence of the relative values of the characteristic times for drying and for glassy skin formation on the development of the instabilities.

The experiments have been performed with concentrated solutions of the hydrosoluble polysaccharide dextran (Sigma Aldrich Chemical Company). Two molecular weights are used: 37 500 and 77 000 g/mol; no difference is found between the two samples. The solutions are prepared by dissolving a given quantity of polymer in ultrapure water (quality milli-ρ). The polymer concentration is kept constant: $\omega_{p0}=0.40$ g/g.

The glass transition temperature of our polymer samples (determined by differential scanning calorimetry) is $220 \pm 10\,^{\circ}$C. For a polymer solution, it increases strongly with the polymer concentration, varying from that of the pure solvent to that of the pure polymer [7]. Thus, at a given temperature T_{expt} the solution has a lower glass transition temperature than T_{expt} for low polymer concentrations and a higher glass transition temperature than T_{expt} for high polymer concentrations. Hence a concentration ω_{pg} exists such that the solution is fluid when $\omega_p < \omega_{pg}$ and glassy when $\omega_p > \omega_{pg}$. During the drying process, due to solvent removal, the polymer concentration increases and the solution, which is initially fluid, becomes glassy.

The drops are deposited onto horizontal glass microscope slides. Before use they are carefully cleaned, kept dehydrating in an oven at 140 °C for a more or less long time (ranging between a few minutes and a few days), and let cool just before use. This thermal treatment allows the contact angle to be varied, in a wide range, from $\theta_0 = 10°$ to 80°. To study variations of the drop shape, both lateral and top views are simultaneously recorded using charge-coupled device cameras. The setup is placed inside a glove box (1.5 m^3) in which the relative humidity is controlled ($\rho = n_{w\infty}/n_{w\mathrm{sat}}$ where $n_{w\infty}$ and $n_{w\mathrm{sat}}$ are the water concentrations in air, respectively, at infinity and at saturation; n_w is expressed in moles per unit volume); $T = 22 \pm 2\,^{\circ}$C, and ρ has been varied between 20 and 80%.

The first profile measured just after drop deposition allows the determination of the initial drop characteristics: R_0 the radius of the contact base, θ_0 the contact angle, and H_0 the apex height. Profiles measured at different times are superposed after normalization by R_0 and H_0. They are also used to calculate the volume V and the vapor/drop interface area S at different times. Spatiotemporal diagrams are also constructed to measure the drop apex height as a function of time.

Two types of evolution are displayed in Fig. 1. In the stable case [Fig. 1(a)], the drop progressively flattens; the apex height regularly decreases while the drop base radius remains constant. At the end of the drying process, a flat ''pancake'' is formed [picture 1(a)]. On the contrary, in the unstable case [Fig. 1(b)], large distortions are observed: after a regular decrease, the apex height quickly increases and may reach a final value which exceeds the initial one. The drop base radius is also constant. At the end, the drop has the shape of a ''Mexican hat'' [picture 1(b)]. So, in both cases, the radius of the drop base remains constant; as was previ-

*Corresponding author. Email address: allain@Fast.u-psud.fr

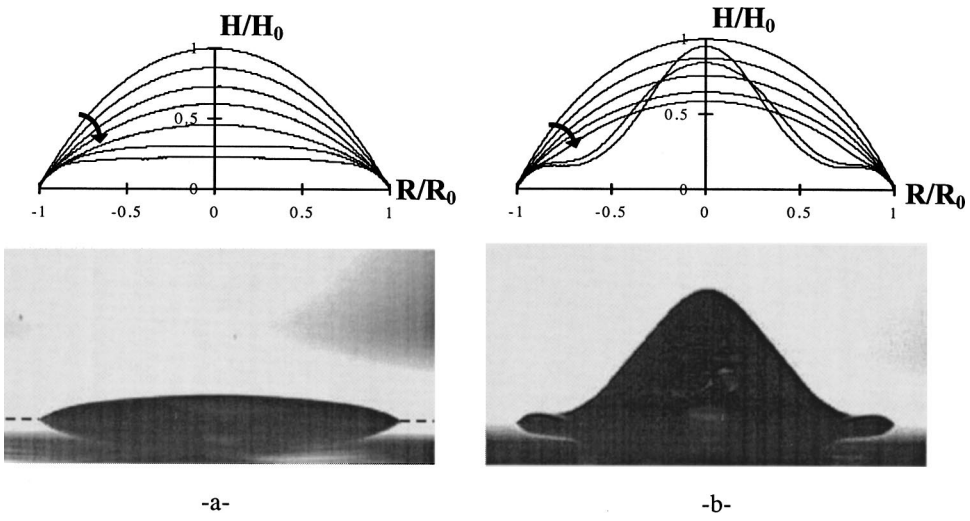

FIG. 1. Top: Superposition of dimensionless profiles of sessile drops of dextran solutions recorded at different times during desiccation ($\rho=50\%, \omega_p=0.40$ g/g). The time elapsed between two consecutive profiles is 180 s. $\theta_0=$ (a) 30° and (b) 40°. Bottom: Side views of the drops at the end of the desiccation: (a) the drop forms a flat "pancake," and (b) a typical "Mexican hat" is displayed ($R_0\cong 2$ mm).

ously observed for colloidal suspensions [8], the polymer deposition and adhesion lead to a strong pinning of the three-phase line, which thus cannot move any more. The apex height variations are, however, markedly different, as shown by the whole profile evolution and the final drop shape.

In order to determine unambiguously whether the evolution of a drop is stable or unstable we measure the variations of the apex height as a function of time (see Fig. 2). The time is normalized by the characteristic time t_D for drying, which is defined from the variation of the drop volume versus time: $t_D^{-1}=-(1/V_0)(\partial V/\partial t)_{t=0}$. Experimentally, the volume is found to decrease linearly with time except near the end of the drying process where the volume decrease slows down [6]. In practice, t_D is the time needed for the complete desiccation of a pure water drop in the same conditions; the accuracy on t_D is $\pm 25\%$. As shown in Fig. 2, for $\theta_0=30°$,

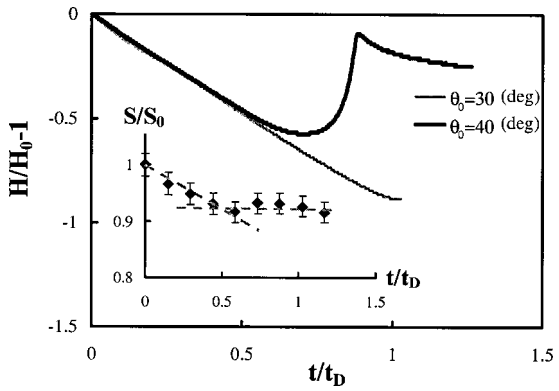

FIG. 2. Dimensionless variations of apex height (H/H_0-1) versus time (t/t_D) for the two drops of Fig. 1. For $\theta_0=30°$, the apex height decreases steadily with time up to $t/t_D\cong 1$: no instability occurs. For $\theta_0=40°$, after a similar decrease, H/H_0 starts increasing and, later, after a steep increase can reach a value that can exceed 1. The time t_B that corresponds to the beginning of the instability is defined as the time at which the decrease of H/H_0-1 vs time begins to differ from the regular decrease. Inset: Dimensionless variations of the drop surface area (S/S_0) versus time (t/t_D) for $\theta_0=40°$. Before the beginning of the instability, a steady decrease takes place while, for $t>t_B$, S/S_0 is constant.

the apex height regularly decreases with time up to $t/t_D\cong 1$; this corresponds to a stable case. On the contrary, for $\theta_0=40°$, which corresponds to an unstable case, the variation of $(H-H_0)/H_0$ with time is at first similar to that observed in the stable case, and then quickly increases. We define the characteristic time t_B for the beginning of the instability as the time at which the decrease of $(H-H_0)/H_0$ versus time begins to differ from the regular decrease. t_B/t_D is always smaller than 1; the accuracy on t_B is $\pm 20\%$.

Stable and unstable situations also differ in the drop/vapor interface area evolutions. In stable cases, S regularly decreases until the final drying stage where it reaches a value close to the substrate/drop contact base area [for the drop corresponding to Fig. 1(a) $S/S_0\cong 0.91$ compared to 0.93]. In the unstable cases, S stops decreasing at a time which corresponds to t_B and remains constant thereafter (see the inset in Fig. 2); S is then significantly larger than the contact base area ($S/S_0\cong 0.93$ compared to 0.88). This difference is related to the mechanism of the instability. Indeed, in the unstable case, the outer layer of the drop becomes glassy at t_B and behaves then like an elastic skin which slows down the evaporation but does not block it due to solvent diffusion through the glassy layer. Thus, the surface area remains constant while the enclosed volume still decreases. A buckling instability takes place to allow for the decrease of the enclosed volume in spite of such constraints as the constant base radius and the skin rigidity. To demonstrate the existence of this glassy skin, a simple test is performed that consists in sucking the drop using a micropipette. If the test is performed during the first stage of the drying process, no solid skin is observed in the central part of the drop, which can be entirely sucked up (only a solid ring along the three-phase line remains on the substrate). On the contrary, no solution can be sucked up after the onset of the instability. This simple test shows that the instability is induced by the formation of a solid skin at the drop surface.

Using the $(H-H_0)/H_0$ vs time curves, which allow an unambiguous determination of the onset of the instability, we have studied the influence of several parameters on the drop evolution. Note first that the nature of the evolution is independent of the initial drop volume; for instance, for ρ

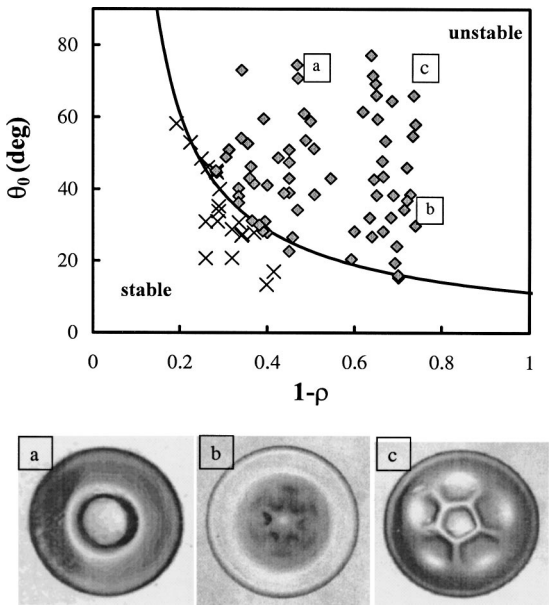

FIG. 3. Top: Diagram showing the different behaviors displayed following the initial contact angle (θ_0) and the humidity rate ($1-\rho$): ×, stable evolutions; ♦, unstable ones. Note that very small or large humidity rates ($\rho<20\%, \rho>80\%$) and contact angles lower than 10° are not accessible with our experimental setup. A good agreement is observed with theoretical predictions [full line, Eq. (3)]. Bottom: Top views at end of the desiccation ($R_0 \cong 2$ mm). (a) $\theta_0 \cong 70°$, $\rho \cong 50\%$: the drop keeps its axisymmetry and a circular fold forms resulting in a dip at the center. (b) $\theta_0 \cong 30°$, $\rho \cong 30\%$: a peak first forms at the drop center, and later radial wrinkles build up that break the axisymmetry. (c) $\theta_0 \cong 70°$, $\rho \cong 30\%$: a complex pattern progressively builds up involving a cascade of buckling, and in the final state the drop axisymmetry is broken.

$=55\%$ and $\theta_0=40°$, when V_0 is varied from 2 to 20 mm^3 an unstable behavior is always observed. The results are reported in the diagram of Fig. 3 in which θ_0 is displayed versus $1-\rho$. Two domains can be clearly identified: at large ρ and small θ_0, no instability develops while at small ρ and large θ_0, instability develops.

In order to predict the onset of the instability, we first need to derive the expressions for the characteristic times t_D and t_B. Assuming that the instability develops when $t_B/t_D < 1$ allows us to determine the limit of the stability domain. Let us first consider the characteristic drying time t_D. Under our experimental conditions (absence of convection in the vapor), the transfer of water in air is limited by diffusion and thus t_D can be written as [8]

$$t_D=\frac{1}{W_{E0}}\frac{V_0}{S_0}=\left(\frac{1}{D_w}\frac{n_1}{n_{wsat}}\right)\frac{K(\theta_0)}{(1-\rho)}R_0^2, \tag{1}$$

where W_{E0} is the water flux in the vapor at the drop/air interface, D_w the diffusion coefficient of water in air, and n_1 the number of water moles per unit volume in liquid water. For a solution, the value of the water concentration in air at saturation is smaller than the value n_{wsat} for pure water. However, for polymer solutions, in the experimental concentration range, only a small difference between the two values is expected (less than 10%) [10]; that justifies the use of n_{wsat} in Eq. (1). The numerical factor $K(\theta_0)$ is the ratio of two terms: $K(\theta_0)=B(\theta_0)/A(\theta_0)$. The factor $A(\theta_0)$, which is related to the shape of the isoconcentration curves of water in air, varies only slightly with θ_0 [11]. On the contrary, the geometrical factor $B(\theta_0)=V_0/(R_0S_0)$ strongly increases with increasing θ_0. So t_D depends on the contact angle, the relative humidity, and the contact base radius. At constant θ_0 and ρ, t_D scales as R_0^2 in good agreement with previous experiments [6]. The variations of t_D/R_0^2 as a function of $1-\rho$ are displayed in Fig. 4. On a log-log plot, the points fall on a straight line with a slope -1 in agreement with Eq. (1). Furthermore, knowing the values of the different quantities involved in Eq. (1) [9,11], we can compute the prefactor, which agrees well with the experimental data (see Fig. 4).

Let us now consider the characteristic time t_B and assume that the instability begins when the drop outer layer becomes glassy. A more complete calculation would also consider that the stress on the skin has to overcome a critical value to lead to the buckling instability [1]. In practice, the mechanical stresses generated by the decrease of volume due to evaporation increase quickly. The stress can be assumed to exceed the critical value for buckling almost as soon as the skin is formed.

To evaluate the polymer concentration at the drop surface, let us express the conservation of the water fluxes at the drop/air interface as $W_E=D_m\nabla\varphi_p$ where D_m is the polymer/solvent mutual diffusion coefficient and φ_p the local polymer volume fraction. The order of magnitude of $\nabla\varphi_p$ is $\nabla\varphi_p \cong (\varphi_{ps}-\varphi_{p0})/\sqrt{D_m t}$, where φ_{ps} and φ_{po} are the values of

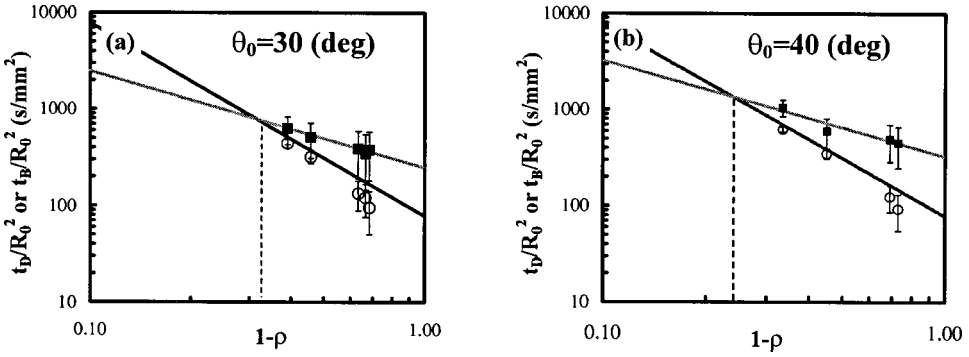

FIG. 4. Variations of t_D/R_0^2 (■) and of t_B/R_0^2 (○) versus $1-\rho$ for two values of $\theta_0=$(a) 30° and (b) 40°. The full lines correspond to the theoretical model: gray lines, Eq. (1), and black lines, Eq. (2).

φ_p, respectively, at the drop surface and in the drop core (assumed to be equal to its value at $t=0$). Setting $\varphi_{ps}=\varphi_{pg}$ at t_B,

$$t_B=\frac{D_m(\varphi_{pg}-\varphi_{p0})^2}{W_{E0}^2}=\left[\frac{D_m(\varphi_{pg}-\varphi_{p0})^2}{D_w^2}\left(\frac{n_1}{n_{w\mathrm{sat}}}\right)^2\right]\frac{1}{A(\theta_0)^2}\frac{1}{(1-\rho)^2}R_0^2. \quad (2)$$

As expected, t_B increases when the evaporation rate decreases, i.e., when R_0 or ρ increases. As for t_D, t_B scales as R_0^2 [6]. Figure 4 displays the variations of t_B/R_0^2 as function of $1-\rho$ for two contact angles. The continuous line drawn in full corresponds to Eq. (2); a good agreement is observed both for the exponent and for the prefactor (D_m is taken equal to 4.3×10^{-10} m^2/s [12] and $\varphi_{pg}=0.51$, i.e., $\omega_{pg}\cong0.62$ g/g).

Assuming that the limit of the stability domain is given by $t_B=t_D$ leads to

$$A(\theta_0)B(\theta_0)=\left(\frac{D_m(\varphi_{pg}-\varphi_{p0})^2}{D_w}\frac{n_1}{n_{w\mathrm{sat}}}\right)\frac{1}{(1-\rho)}. \quad (3)$$

Note first that Eq. (3) does not involve R_0; so, at constant θ_0 and ρ, the type of the drop evolution will not depend on the drop volume, which agrees well with our observations. In Fig. 3, the black continuous line is calculated from Eq. (3) using the same values for the various quantities as in Fig. 4; a fairly good agreement is observed with the experimental results.

Depending on the experimental conditions, various patterns are observed, in which the drop axisymmetry is or is not broken [5]. First, for an intermediate relative humidity ($\rho\cong50\%$), only the primary instability takes place and the drop shape remains symmetrical. The shape depends, however, on the contact angle: for a low contact angle ($\theta_0=40°$), the drop displays a peak [Fig. 1(b)], while for a large contact angle ($\theta_0=70°$) a trough builds up on the drop axis [Fig. 3(a)]. For small relative humidity ($\rho\cong30\%$), secondary instabilities occur. For a low contact angle ($\theta_0=30°$), after the increase of the apex height, the top views show a breaking of the drop axisymmetry with the formation of radial wrinkles [Fig. 3(b)]. The number of these wrinkles (here, 6) increases with R_0. For a large contact angle ($\theta_0=70°$) a complex pattern progressively builds up involving a cascade of buckling [Fig. 3(c)] that breaks the drop axisymmetry. So, depending on the contact angle and relative humidity, the distortions of the shape induced by the instability are different, and for large evaporation rates (low ρ) secondary instabilities occur. These various types of shapes are closely related to different modes of buckling instability.

In summary, we have demonstrated that the large shape distortions displayed during drop drying are related to a buckling instability. The comparison of the characteristic times for drying and for glassy skin formation gives a good description of the results and in particular allows for the prediction of the occurrence of the instability. The final drop shapes can be explained by assuming a close relation with the buckling of thin solid sheets.

We thank Professor L. Mahadevan and Professor J. P. Hulin for useful discussions and G. Calligari and F. Wendling for their help in the experiments.

[1] S. Timoshenko and J. M. Gere, *Theory of Elastic Stability*, 2nd ed. (McGraw-Hill, New York, 1961).
[2] R. Lipowski, Nature (London) **349**, 475 (1991); R. Lakes, *ibid.* **414**, 503 (2001); D. Drasdo, Phys. Rev. Lett. **84**, 4244 (2000).
[3] F. Cleymand, C. Coupeau, J. Colin, and J. Grilhé, Eur. Phys. J.: Appl. Phys. **10**, 3 (2000); J. W. Hutchinson, M. D. Thouless, and E. G. Liniger, Acta Metall. Mater. **40**, 295 (1992); J. Möller, D. Reiche, M. Bobeth, and W. Pompe, Surf. Coat. Technol. **150**, 8 (2002); B. Audoly, Phys. Rev. Lett. **83**, 4124 (1999); B. Audoly, A. Pocheau, and B. Roman, Eur. Phys. J. B **27**, 7 (2002).
[4] L. Pauchard, F. Parisse, and C. Allain, Phys. Rev. E **59**, 3737 (1999).
[5] L. Pauchard and C. Allain, C.R. Physique **4**, 231 (2003).
[6] L. Pauchard and C. Allain, Europhys. Lett. **62**, 897 (2003).
[7] D. J. Plazek and K. L. Ngai, in *Physical Properties of Polymer Handbook* (AIP, Woodbury, NY, 1996), Chap. 12.
[8] E. Adachi, A. S. Dimitrov, and K. Nagayama, Langmuir **11**, 1057 (1995); F. Parisse and C. Allain, J. Phys. II **6**, 1111 (1996); R. D. Deegan, O. Bakajin, T. F. Dupont, G. Huber, S. R. Nager, and T. Witten, Nature (London) **389**, 827 (1997).
[9] F. P. Incropera and D. P. De Witt, *Fundamentals of Heat and Mass Transfer* (Wiley, New York, 1990).
[10] P. G. de Gennes, *Scaling Concepts in Polymer Physics* (Cornell University Press, Ithaca, NY, 1979).
[11] R. G. Picknett and R. Bexon, J. Colloid Interface Sci. **61**, 336 (1977).
[12] For most polymer solutions, D_m ranges between 10^{-10} and 10^{-9} m^2/s; see, for instance, M. Doi and S. F. Edwards, *The Theory of Polymer Dynamics* (Clarendon, Oxford, 1986).